Biomaterials 227 (2020) 119556

Contents lists available at ScienceDirect

Biomaterials

journal homepage: www.elsevier.com/locate/biomaterials

Engineered antibody-functionalized porous silicon nanoparticles for therapeutic targeting of pro-survival pathway in endogenous neuroblasts after stroke

Vimalkumar Balasubramanian[a,*****,1], Andrii Domanskyi[c,**,1], Juho-Matti Renko[d], Mirkka Sarparanta[e], Chang-Fang Wang[a,***], Alexandra Correia[a], Ermei Mäkilä[f], Osku S. Alanen[e], Jarno Salonen[e], Anu J. Airaksinen[e], Raimo Tuominen[d], Jouni Hirvonen[a], Mikko Airavaara[c,****,2], Hélder A. Santos[a,b,*,2]

[a] Drug Research Program, Division of Pharmaceutical Chemistry and Technology, Faculty of Pharmacy, University of Helsinki, FI-00014, Finland
[b] Helsinki Institute of Life Sciences, HiLIFE, University of Helsinki, FI-00014 Finland
[c] Institute of Biotechnology, HiLIFE, University of Helsinki, FI-00014, Finland
[d] Drug Research Program, Division of Pharmacology and Pharmacotherapy, Faculty of Pharmacy, University of Helsinki, FI-00014, Finland
[e] Department of Chemistry, Radiochemistry, University of Helsinki, FI-00014, Finland
[f] Department of Physics and Astronomy, Laboratory of Industrial Physics, University of Turku, FI-20520, Finland

HIGHLIGHTS

- Porous silicon nanoparticles are conjugated with an antibody (anti-PSA-NCAM-PE) for targeting neuroblasts in the brain.
- Akt pathway activator SC-79 is delivered to neuroblasts by anti-PSA-NCAM-PE-PSi-conjugated porous silicon nanoparticles to promote proliferation of neuroblasts for neuron regeneration.
- The Akt signaling pathway is increased by the conjugated nanoparticles in doublecortin positive neuroblasts both in cultured cells and *in vivo* in the rat brain.
- The conjugated nanoparticles are a novel tool for future studies to develop new therapeutic strategies, aiming at regenerating functional neurocircuitry after stoke.

ARTICLE INFO

Keywords:
Porous silicon nanoparticles
Targeting neuroblasts
Akt pathway activation
Neuron regeneration
Antibody bioconjugation

ABSTRACT

Generation of new neurons by utilizing the regenerative potential of adult neural stem cells (NSCs) and neuroblasts is an emerging therapeutic strategy to treat various neurodegenerative diseases, including neuronal loss after stroke. Committed to neuronal lineages, neuroblasts are differentiated from NSCs and have a lower proliferation rate. In stroke the proliferation of the neuroblasts in the neurogenic areas is increased, but the limiting factor for regeneration is the poor survival of migrating neuroblasts. Survival of neuroblasts can be promoted by small molecules; however, new drug delivery methods are needed to specifically target these cells. Herein, to achieve specific targeting, we have engineered biofunctionalized porous silicon nanoparticles (PSi NPs) conjugated with a specific antibody against polysialylated neural cell adhesion molecule (PSA-NCAM). The PSi NPs loaded with a small molecule drug, SC-79, were able to increase the activity of the Akt signaling pathway in doublecortin positive neuroblasts both in cultured cells and *in vivo* in the rat brain. This study opens up new possibilities to target drug effects to migrating neuroblasts and facilitate differentiation, maturation and survival

* Corresponding author. Drug Research Program, Division of Pharmaceutical Chemistry and Technology, Faculty of Pharmacy, University of Helsinki, FI-00014 Finland
** Corresponding author.
*** Corresponding author.
**** Corresponding author.
***** Corresponding author.
E-mail addresses: vimalkumar.balasubramanian@helsinki.fi (V. Balasubramanian), andrii.domanskyi@helsinki.fi (A. Domanskyi), chang-fang.wang@helsinki.fi (C.-F. Wang), mikko.airavaara@helsinki.fi (M. Airavaara), helder.santos@helsinki.fi (H.A. Santos).
[1] These authors contributed equally to this work.
[2] These authors share the equal contribution to the work.

https://doi.org/10.1016/j.biomaterials.2019.119556
Received 12 August 2019; Received in revised form 4 October 2019; Accepted 15 October 2019
Available online 18 October 2019

of developing neurons. The conjugated PSi NPs are a novel tool for future studies to develop new therapeutic strategies aiming at regenerating functional neurocircuitry after stoke.

1. Introduction

The striking discovery of adult neurogenesis has uplifted the hope for generating new neurons in the adult brain to restore the brain and its functions after injuries or neurodegeneration [1,2]. In principle, multi-potent self-renewing neural stem cells (NSCs) present in a germinal niche, such as the subventricular zone (SVZ) have the potential to replace or repair the damaged neurons that can positively impact the treatment of brain injuries or neurodegenerative diseases [3,4]. There is a great demand for utilizing the regenerative potential of NSCs to modulate their differentiation and survival to replace dead neurons for therapeutic purposes [5,6]. In this direction, new therapeutic strategies are needed to directly stimulate the endogenous NSCs and/or committed neuronal progenitors (neuroblasts) *in situ* and enhance their survival [7,8], particularly in stroke where survival of migrating neuroblasts is the limiting factor [9,10]. To attain an efficient biological or therapeutic response, effective and selective delivery of bioactive molecules to targeted migrating neuroblasts is one of the main prerequisites. To achieve this, nanoparticles (NPs) can be a promising platform for selective cell targeting and modulation of the fate of NSCs [11–13]. Although large arrays of NPs have been developed for targeted drug delivery [14–16], including for the brain [17], applications in neuronal differentiation/neurogenesis are scarce [18]. For example, it has been reported that polymeric NPs loaded with retinoic acid can stimulate neurogenesis *in vivo* through the controlled, intracellular release of retinoic acid from NPs in SVZ [19]. However, in this study NPs

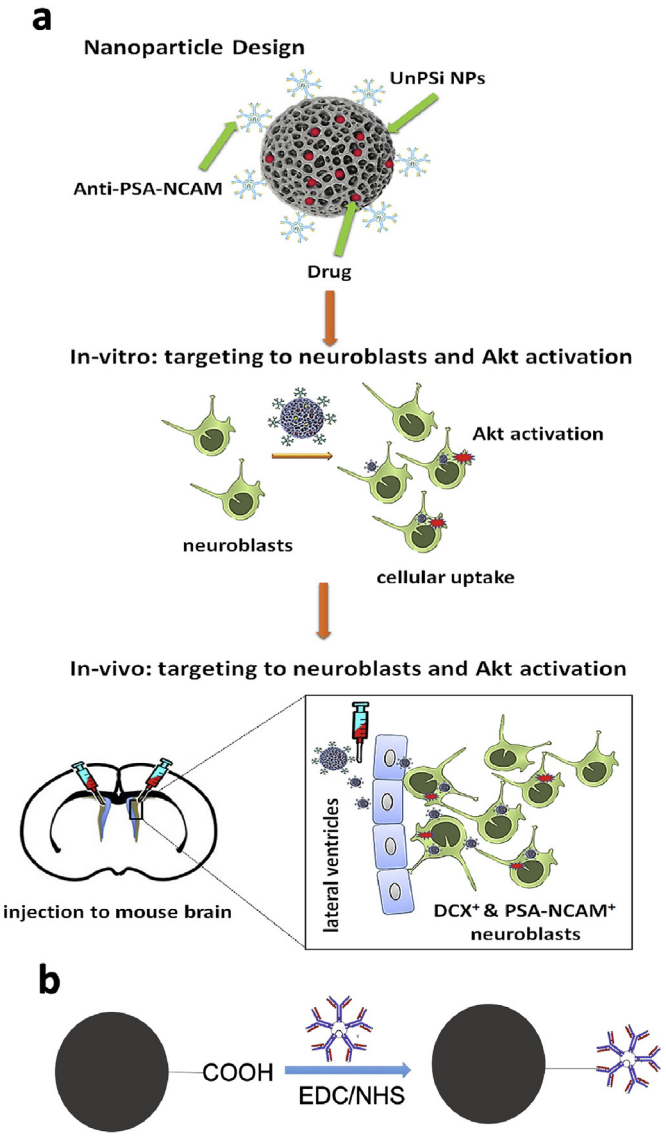

c

Sample name	Size in diamater (nm)	PDI	Surface charge (mV)
UnPSi	176 (± 1)	0.07 (± 0.02)	-27 (± 1)
Anti-PSA-NCAM-UnPSi (Conjugated)	358 (± 3)	0.23 (± 0.01)	-19 (± 4)
Anti-PSA-NCAM-UnPSi (Physical mix)	204 (± 2)	0.17 (± 0.02)	-25 (± 1)

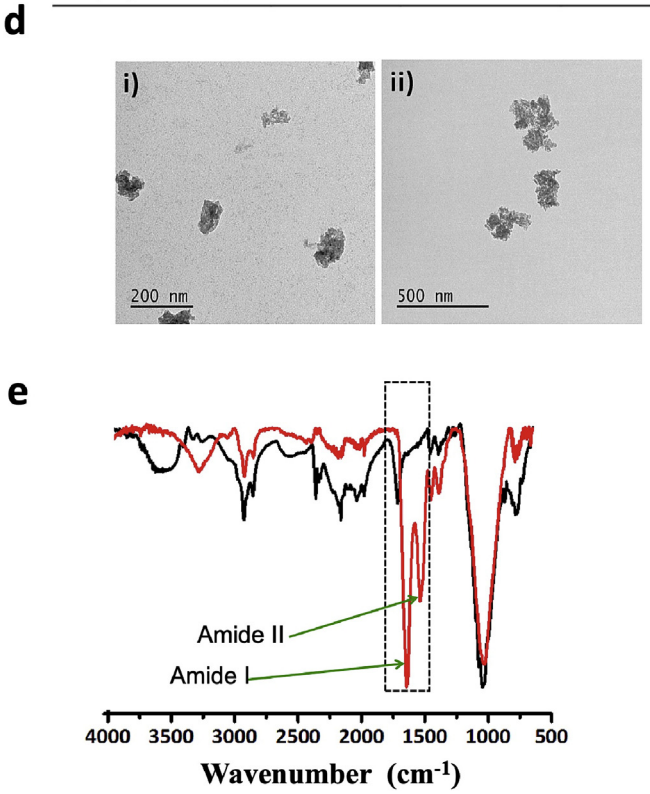

Fig. 1. Physicochemical characterization of developed anti-PSA-NCAM-PE-UnPSi NPs. (a) Schematic representation of anti-PSA-NCAM-PE conjugated UnPSi NPs loaded with a small molecule drug to target endogenous DCX^+ and $PSA\text{-}NCAM^+$ neuroblasts and activate the Akt signaling pathway to enhance cell survival both *in vitro* and *in vivo*. (b) Surface functionalization scheme. (c) Particle size, PdI and zeta (ζ)-potential of UnPSi NPs, before and after conjugation with anti-PSA-NCAM-PE antibody and in simulated conjugation condition (physical mixing). (d) Representative TEM images of UnPSi NPs before (i) and after conjugation with anti-PSA-NCAM-PE (ii). (e) ATR – FTIR analysis of UnPSi NPs (black line) and anti-PSA-NCAM-PE-UnPSi (red line). Dotted lines indicate the shift in the bands that corresponds to conjugation. (For interpretation of the references to colour in this figure legend, the reader is referred to the Web version of this article.)

were not targeted to any specific type of neural lineage cells, instead it was reported to achieve intracellular drug release non-selectively in different cell types in and around the SVZ. To the best of our knowledge, so far only one NP-based system has been developed to target endogenous NSCs *in vivo*, mainly due to the lack of specific targeting moieties. In this recent study, it was shown that lipid capsules adsorbed with neurofilament-derived peptides (NFL-TBS.40–63), which were reported to selectively interact with NSCs in the SVZ, were able to target the endogenous NSCs *in vivo* [20]. However, the biological or therapeutic significance of this targeting system has not been reported and the limited survival of migrating neuroblasts after stroke remains.

Adult neurogenesis is a finely regulated multistep process that involves the proliferation of NSCs and transit-amplifying cells, migration and differentiation of neuroblasts, and integration of newly differentiated neurons into already existing neuronal circuitries [21,22]. NSCs can differentiate into several classes of neural lineage cells, including astrocytes and oligodendrocytes [23]. Hence, directing *in vivo* differentiation of endogenous NSCs into specific neural lineage cells, particularly into neurons, is difficult to achieve. Moreover, due to their high proliferative potential, stimulation of NSCs *in vivo* may potentially facilitate carcinogenesis, which raises the concern for clinical applications [24,25]. Unlike NSCs, neuroblasts are committed neuronal progenitors with limited proliferation potential. Neuroblasts are characterized by the expression of doublecortin (DCX^+) and cell surface glycoprotein polysialylated neural cell adhesion molecule ($PSA\text{-}NCAM^+$) [26,27]. Furthermore, increased expression of DCX in neuroblasts is known to enhance their migration and at the same time limit their proliferation [28]. Therefore, developing targeted NPs using an anti-PSA-NCAM antibody as a ligand for endogenous neuroblasts, followed by loading bioactive molecules to promote their survival and differentiation, can support the generation of new neurons (Fig. 1a). In this study, we demonstrate that targeted anti-PSA-NCAM antibody-conjugated NPs successfully bind neuroblasts both *in vitro* and *in vivo*. The novelty of our study lies in the anti-PSA-NCAM antibody-conjugated NPs that show specificity to neuroblast targeting. Moreover, we demonstrate the *in vivo* activation of the Akt pathway after intraventricular injection of targeted NPs loaded with an Akt stimulating drug SC-79 [29]. To test our hypothesis regarding the design and characterization of drug loaded, antibody conjugated NPs, we selected porous silicon (PSi) NPs, a versatile drug delivery platform, which can readily accommodate a wide range of payloads, tunable with surface chemistry to allow biofunctionalization, biocompatible, and biodegradable as favorable biological properties [30–32]. PSi NPs are highly degradable at pH > 7 and the degradation of PSi is highly dependent on the porosity of the NPs. Thus, in the brain, it will take few days for the PSi NPs to degrade to non-toxic silicic acid [33]. Our results on the toxicity of PSi NPs demonstrate their safety and biodegradability in different cell culture conditions and *in vivo* [31,32,34].

2. Materials and methods

2.1. Fabrication of undecylenic acid thermally hydrocarbonized PSi (UnPSi) NPs

Monocrystalline boron doped p + Si ⟨100⟩ wafers with 0.01–0.02 Ω cm of a resistivity were electrochemically anodized in a 1:1 (v/v) hydrofluoric acid (38%)-ethanol electrolyte, pulsed with alternating low and high current density etching profiles to create fracture planes into the porous layer at periodic intervals. Afterwards, the etching current was increased to the electropolishing region to lift off the obtained multilayer film from the substrate. The films were dried and placed under N_2 flow (1 L min^{-1}) for 30 min at room temperature to eliminate oxygen and residual moisture. At room temperature, acetylene (C_2H_2) flow (1 L min^{-1}) was added to the N_2 flow for 15 min before increasing the temperature for 15 min to 500 °C under the 1:1 (v/v) N_2/C_2H_2 flow. The PSi (THCPSi) films were then allowed to cool down to room temperature under N_2 flow and further treated by immersion in undecylenic acid for 16 h at 120 °C to provide a carboxyl functionalization (UnPSi). The NPs were produced by ball milling the UnPSi films in 10 vol-% undecylenic acid-decane solution and the particle size selection was done by centrifugation.

2.2. Physicochemical characterization of the nanoparticles

Dynamic and electrophoretic light scattering (DLS and ELS). The hydrodynamic diameter (*Z*-average), polydispersity index (PDI), and ζ-potential of the NPs were determined by DLS and ELS using a Zetasizer Nano ZS instrument (Malvern Instruments Ltd). The measurements were performed in Milli-Q water and PBS at a NP concentration of ~25 μg ml^{-1}.

Fourier transform infrared (FTIR) spectroscopy. The surface chemistry of the dry NPs was evaluated by ATR-FTIR using a Bruker VERTEX 70 series FTIR spectrometer (Bruker Optics, Germany) and an ATR sampling accessory (MIRacle, Pike Technology, Inc.). The ATR–FTIR spectra were recorded in the wavenumber region of $4000-500\ cm^{-1}$ with a resolution of 4 cm^{-1} at room temperature using OPUS 5.5 software.

Transmission electron microscopy (TEM). The NPs were first dispersed in Milli-Q water, and dropped onto plasma treated, carbon (C)-coated copper TEM grids, followed by staining with 2% uranyl acetate. The samples were allowed to dry overnight at room temperature before analysis and images were acquired using Tecnai TEM.

2.3. Bioconjugation

The fabricated UnPSi NPs were covalently conjugated to anti-PSA-NCAM antibody labeled with PE (anti-PSA-NCAM-PE, Miltenyi Biotec, Germany) in the 1:10 (w/w) ratio of anti-PSA-NCAM:UnTHCPSi using a 1-ethyl-3-(3-dimethylaminopropyl) carbodiimide hydrochloride/N-hydroxysulfosuccinimide (EDC/NHS) chemistry. Briefly, 200 μg of UnPSi NPs was suspended in 400 μL of 10 mM 2-(N-morpholino)ethanesulfonic acid (MES; pH 5.5), containing 10 mM of EDC and 10 mM of NHS. The reaction was carried out for 1.5 h at room temperature with continuous stirring to activate the carboxyl groups on the surface of UnPSi NPs. The activated NPs were exposed to 20 μg of anti PSA-NCAM-PE in PBS (pH 7.2) with stirring overnight in the dark at room temperature, and anti PSA-NCAM-PE-UnPSi NPs were washed with PBS (pH 7.2). After washing steps through centrifugation, the amount of antibody conjugated onto the surface of the PSi NPs was determined by fluorescence analysis, using a fluorescence spectrometer (VarioskanTM LUX Multimode Microplate Reader, Thermo Fisher Scientific). To determine the conjugation efficiency, the fluorescence of antibody-conjugated NPs was measured against the established standard calibration curve of predetermined concentration of free anti PSA-NCAM-PE. In addition, the average number of antibody to each PSi NP is calculated as follows:

The amount of the antibody conjugated to 100 μg of the nanoparticles = 4.66 μg.

Mw of the antibody = 900 000 Da.

Molarity of the antibody = $\frac{4.66 * 10^{-6}}{900\,000} = 5.18 \times 10^{-12}$ mol.

Molarity of the antibody: 1 mol = Avogadro's number = 6.02×10^{23}

The number of the antibody conjugated to 100 μg of the nanoparticles:

$= (5.18 \times 10^{-12}) \times (6.02 \times 10^{23}) = 3.12 \times 10^{12}$

The number of the PSi NPs in 100 μg of the particles (considering spherical shape) = 4.31×10^{10}

The average number of antibody conjugated to each nanoparticle = $\frac{3.12 \times 10^{12}}{4.31 \times 10^{10}} = 72.39$.

2.4. Drug loading, determination of loading degree

Drug loading and determination of loading degree (LD). UnPSi NPs or anti-PSA-NCAM-PE-conjugated UnPSi NPs (200 μg) were suspended in 1 ml of DMSO: ethanol (1:9 ratio) mixture, containing 2 mg ml^{-1} of SC-79 (Tocris Bioscience, #4635) drug and stirred for 2 h at room temperature. Next, the sample was washed with Milli-Q water by centrifuging at 13 000 rpm for 5 min and excess unloaded drug in supernatant was removed. The washing procedure was repeated thrice to remove the unloaded SC-79 drug. Then, the NPs were suspended in ethanol and stirred at room temperature for 1 h. After centrifugation, supernatant was collected and analyzed in high-performance liquid chromatography (HPLC) to determine the amount of SC-79 loaded in Un-PSi NPs and calculate the loading degree of SC-79 using the established standard calibration curve of predetermined concentration of free SC-79.

High-performance liquid chromatography (HPLC). An Agilent 1100 series HPLC system (Agilent Technologies, Germany) was used to quantify the SC-79 compound loaded into the UnPSi NPs. A Gemini − NX 3 μm C_{18} 110 A reversed phase column (100 × 4.6 mm, Phenomenex, USA) was used. The mobile phase was 0.2% trifluoroacetic acid (pH 2.0) and acetonitrile (ratio of 50:50 v/v), the flow rate was 0.8 mL/min, the injection volume was 20 μL, and the wavelength was 272 nm.

2.5. Iodine-125 radiolabeling of anti-PSA-NCAM-PE-UnPSi NPs for ex vivo biodistribution study

Anti-PSA-NCAM-PE-UnPSi NPs (240–300 μg) at a 1 mg ml^{-1} concentration in 1 × PBS (pH 7.2) were added into a 1.5-ml microtube with 10 μl of 1 × PBS (pH 7.4), 47.5–54.2 MBq of $Na^{125}I$ in 10^{-5} M NaOH, pH 10 (PerkinElmer, Boston, MA, USA) and 10 μl of chloramine-T solution (7 mg ml^{-1}). The sample was incubated for 30 min at room temperature with careful mixing periodically on a vortex mixer. Then 50 μL of ascorbic acid solution (20 mg ml^{-1}) was added to quench the reaction. The tube was centrifuged at 13 200 rpm for 10 min and the supernatant was removed. The NPs were purified with two consecutive washes with 1 × PBS (pH 7.4) with dispersal of the NP pellet with sonication on an ultrasonic tip in between. Radiochemical purity of the ^{125}I-labeled NPs was confirmed with paper chromatography using 1 × PBS (pH 7.4) as the eluent followed by exposure of the chromatographic paper to a phosphorimaging plate (BAS-IP TR2025, GE Healthcare Life Sciences, Marlborough, MA, USA) for digital autoradiography. The ^{125}I-labeled NPs were stored at 4 °C overnight. On the day of the experiment, the radiolabeled NPs were further purified with sonication and wash in 1 × PBS (pH 7.4), collected with centrifugation at 7200 rpm, and resuspended in 1 × PBS (pH 7.4) with sonication. The radiochemical purity of the final formulation was checked with paper chromatography as described previously, and the injected formulation was confirmed to be void of free ^{125}I.

The stability of the ^{125}I radiolabel was measured *in vitro* in the formulation and in 50% human plasma in 1 × PBS (pH 7.4) at 37 °C. For the stability assay, an aliquot of the formulated ^{125}I-labeled anti-PSA-NCAM-PE-UnPSi NPs (93 MBq mg^{-1}) were transferred to the assay media at a final concentration of 240 kBq ml^{-1} and incubated on an orbital shaker for the designated time. At 15, 30, 45, 60, 90, 120, 180, 240, 300, 360, and 1440 min time points, 100 μl samples were drawn and the NPs were collected by centrifugation at 13 200 rpm. The radioactivity retained in the NPs and in the supernatant were measured on an automated gamma counter (1480 Wizard 3″, PerkinElmer, Waltham, MA, USA).

2.6. Animal experiments

NMRI and C57Bl6 mice (Charles River) and male Sprague-Dawley rats (Envigo) were housed in 12-h light-dark cycle with free access to food and water. For collecting the E13.5 embryos, the mice were mated and the morning when the vaginal plug was found was defined as E0.5. All animal experiments were approved by the national Animal Experiment Board of Finland (protocol approval numbers ESAVI/5459/04.March 10, 2011, ESAVI/7812/04.July 10, 2015, KEK16-015).

2.7. Culturing embryonic neuronal stem/progenitor cells (NSPCs)

The telencephalons of E13.5 mouse embryos were isolated and dissociated by trituration. The cells were cultured in neurosphere growth medium containing Dulbecco's Modified Eagle Medium (DMEM)/F12 (Gibco) supplemented with B27 (1 × Gibco, #17504044), epidermal growth factor (EGF, 20 ng ml^{-1}, Gibco), fibroblast growth factor-2 (FGF-2, 20 ng ml^{-1}, Gibco), GlutaMAX (1 × Gibco, #35050038) and penicillin-streptomycin (50 U ml^{-1}, Gibco). After 5–7 days of culture, neurospheres were collected by centrifugation at 200*g* for 5 min. After dissociation by Accutase (Gibco) treatment for 5 min at 37 °C and trituration, the NSPCs were collected by centrifugation at 300*g* for 6 min, resuspended in 1 ml fresh neurosphere medium and filtered through 70 μm filter (Miltenyi Biotech). Approximately 5 × 10^5 NSPCs were transferred to T25 cell culture flask (CellStar) containing 5 ml fresh neurosphere medium. Neurospheres were passaged every 7–10 days; NSPCs from passages 1–2 were used for the experiments.

2.8. Cellular interaction studies by immunofluorescent staining and confocal imaging

For confocal imaging, embryonic neurospheres were dissociated as described above, and NSPCs were seeded at a density of ca. 4 × 10^4 cells per well in 300 μl of neurosphere medium on poly-L-ornithine/laminin-coated Lab-Tek 8-chamber slides (Thermo Fisher Scientific, USA). NSPCs were incubated with fluorescently labeled NPs (non-targeted UnPSi loaded with TRITC and anti-PSA-NCAM-PE-UnPSi) at different doses (25, 50, and 100 μg ml^{-1}) for 9 h or 24 h, as indicated in the text and figure legends. The cells were fixed in 4% paraformaldehyde (PFA) solution in PBS for 20 min at room temperature, washed twice with PBS, and permeabilized for 15 min with PBS containing 0.2% Triton X-100 (PBST) solution. After blocking unspecific antibody binding sites by incubation for 1 h at room temperature in blocking solution (PBST containing 5% normal horse serum (DAKO)), the cells were incubated with the anti-phospho-S6 ribosomal protein (Cell Signaling, #4857; diluted 1:200 in blocking solution), anti-DCX (Santa Cruz Biotechnology, #sc8066; 1:200), anti-nestin (Millipore, #MAB353; 1:500), or anti-PSA-NCAM (Chemicon #MAB5324; 1:500) antibody overnight at 4 °C, washed three times with PBS, and incubated with corresponding AlexaFluor-488 or AlexaFluor-568 conjugated secondary antibodies (Life Technologies; diluted 1:500 in PBST) for 1 h at room temperature. After three washes with PBS the cells were stained with 4′,6-diamidino-2-phenylindole (DAPI, 0.2 μg ml^{-1} in PBS) for 10 min and kept in PBS at 4 °C protected from light until imaging.

The immunostained cells were imaged with Leica TCS SP5II HCS A confocal inverted microscope (Leica Microsystems, Germany) equipped with a 405 Diode laser, argon laser (488 nm) and Helium Neon laser (HeNe 633) and an HCX PL APO 63 × /1.2 W Corr/0,17 CS (water immersion) objective. The obtained images were processed using Fiji image J (1.49c) software.

2.9. Cell viability assay

For the viability assay, NSPCs were seeded at a density of ca. 1.5 × 10^4 cells per well in 100 μl of neurosphere medium on poly-L-ornithine/laminin-coated 96-well plates (CellStar). 24 h after plating, NSPCs were incubated with NPs (non-targeted UnPSi and anti-PSA-NCAM-PE-UnPSi) at different dosses (25, 50, 100 μg mL^{-1}) for 6 h or 24 h. The cell viability was analyzed using CellTiter-Glo® Luminescent Cell Viability Assay (Promega, USA) by measuring the luminescence

using a Varioskan Flash microplate reader (Thermo Fisher Scientific Inc., USA).

2.10. In vivo targeting

2.10.1. Intravenous delivery of iodine-125 -radiolabeled anti-PSA-NCAM-PE-UnPSi NPs in a rat model of stroke

Biodistribution studies were conducted in male Sprague-Dawley (Hsd:SD) rats (8–10 weeks, Envigo, Huntingdon, UK). Ischemic stroke was induced by the transient 60-min ligation of the bilateral common carotid arteries (CAA) and the right middle cerebral artery (MCA) under chloral hydrate anesthesia (10 ml/kg) as described previously [35], and were used for the radiolabeled NP biodistribution study 48 h after the surgery. Operation-naïve Hsd:SD rats were used as controls. ^{125}I-labeled anti-PSA-NCAM-PE-UnPSi NPs were administered intravenously under isoflurane anesthesia (2.5% isoflurane in 40% oxygen in medical air carrier) to a cannulated lateral tail vein. The administered dose was 25 μg of NPs in 200 μl of 1 × PBS (pH 7.4), which yielded radioactivity of 2.2 ± 0.6 MBq (stroke cohort) and 2.2 ± 0.3 MBq (naïve cohort). At 2 h (n = 3 for both cohorts) and 24 h (n = 3 for both cohorts) after administration, the rats were sacrificed by an overdose of pentobarbital and transcardially perfused with 0.9% NaCl followed by 4% PFA. Select tissues, including the infarct and contralateral brain hemispheres, were collected, weighed, and the radioactivity counted on an automated gamma counter. The results are expressed as the percentage of the injected dose per gram of tissue (%ID/g) or for the brain as the differential absorption ratio (DAR) calculated according to the equation:

$$DAR = \frac{Radioactivity\ \ in\ \ tissue\ \ [cpm]}{Mass\ \ of\ \ tissue\ \ [g]} \Big/ \frac{Injected\ \ radioactivity\ \ [cpm]}{Body\ \ weight\ \ [g]}$$

2.10.2. Intraventricular injections

Adult 8–10 weeks old C57Bl6 mice were used for stereotaxic injections of NPs (anti-PSA-NCAM-PE-UnPSi or anti-PSA-NCAM-PE-UnPSi loaded with SC-79) or controls (non-targeted UnPSi, non-targeted UnPSi loaded with TRITC or SC-79, free SC-79, free TRITC, free anti-PSA-NCAM-PE antibody, UnPSi mixed with anti-PSA-NCAM-PE antibody) or vehicle (PBS), as indicated in the text and figure legends. About 5 μl of corresponding solution was injected bilaterally into the lateral ventricles (LVs) at A/P 0.0; M/L ± 0.9; D/V −2.5 mm from the bregma under isoflurane anesthesia at a rate of 1 μl/min and the needle (WPI NanoFil 33G) was retained in place for 2 min after the injection as described elsewhere [10].

2.10.3. Immunofluorescent staining of brain sections

Anaesthetized mice were transcardially perfused with PBS followed by 4% PFA in PBS solution. Brains were dissected, fixed in 4% PFA for 24 h and either immersed to 30% sucrose in PBS for cryosectioning or embedded in paraffin. Brains were cryosectioned into 30 μm-thick free-floating coronal sections, or 5 μm-thick paraffin coronal sections. For immunostaining, paraffin sections were deparaffinized and re-hydrated through a graded alcohol series before being subjected to antigen retrieval in 0.05% citraconic anhydride buffer, pH 7.4, at 100 °C for 10 min.

After blocking unspecific antibody binding sites by incubation for 1 h at room temperature in blocking solution (PBST containing 5% normal horse serum (DAKO)), the sections were incubated with anti-phospho-S6 ribosomal protein (Cell Signaling, #4857; 1:200), anti-DCX (Santa Cruz Biotechnology, #sc8066; 1:200) or anti-Ki67 (Thermo Fisher, #RM-9106-S1; 1:200) antibody in blocking solution at 4 °C overnight. For immunofluorescent staining, the sections were incubated with corresponding AlexaFluor-488 or AlexaFluor-568 conjugated secondary antibodies (Life Technologies; diluted 1:500 in PBST) for 1 h at room temperature. For immunohistochemistry, biotinylated secondary antibody (Vector Laboratories; 1:400) and peroxidase-conjugated streptavidin Vectastain ABC-detection system (Vector Laboratories) were used. Sections were developed with diaminobenzidine peroxidase substrate (Vector Laboratories) and imaged with Pannoramic 250 Flash II slide scanner (3DHistech Ltd, http://www.biocenter.helsinki.fi/bi/histoscanner/index.html).

2.11. Statistical analysis

Statistical significance was calculated by one-way analysis of variance (ANOVA) followed by Holm-Sidak's multiple comparison test. All statistical analyses were performed in GraphPad Prism 8.20 software (GraphPad Software, Inc).

3. Results and discussion

In this work, undecylenic acid modified thermally hydrocarbonized PSi (UnPSi), as studied earlier for other drug delivery applications [32,36–38], was developed to bio-conjugate with targeting ligands. To develop NPs targeting endogenous neuroblasts, we used carbodiimide crosslinking chemistry to covalently link the R-phycoerythrin-conjugated anti-PSA-NCAM antibodies (anti-PSA-NCAM-PE) to the surface of UnPSi NPs (Fig. 1b). The size, size distribution, charge and morphology of the NPs were analyzed by dynamic light scattering, zeta (ζ)-potential measurements and transmission electron microscopy (TEM) (Fig. 1c and d). The results showed that an average particle size of bare UnPSi NPs was 176 nm (polydispersity index, PdI: 0.07, Fig. S1) and the size was increased to 358 nm (PdI: 0.229) for the anti-PSA-NCAM-PE-UnPSi (Fig. 1c, and Fig. S1). A titration modification was tested with different ratios of antibody to NPs (5, 10 and 20 μg of antibody to 200 μg of NPs). The size of the NPs increased gradually by increasing the amount of antibody used to conjugate to the NPs (Table S1 and Fig. S1). Taken into consideration that anti-PSA-NCAM is a large IgM antibody (Mw∼ 900 000 g mol^{-1}, pentameric form) and its physical size can be ∼40 nm [39], the size increase of anti-PSA-NCAM-PE-UnPSi NPs could be due to the surface conjugation of anti-PSA-NCAM-PE. The ζ-potential measurements of bare UnPSi NPs showed highly negative surface charges (−27 mV), whereas the anti-PSA-NCAM-PE-UnPSi NPs showed a decrease in the surface charge to (−19 mV), due to the presence of amine groups in anti-PSA-NCAM-PE (pentameric form of IgM) (Fig. 1c). This indicates the successful conjugation process. We also used the TEM technique to analyze the particle size (Fig. 1d). Due to the contrast of PSi NPs and the antibody, we could only see the PSi NPs in the TEM. In the TEM images, the size of the NPs before and after antibody modification were similar, which is consistent with other studies [40,41]. The physical mixing of anti-PSA-NCAM-PE and UnPSi NPs (simulated conjugation condition/non-conjugated) showed no significant increase in size (204 nm) and minor changes in surface charge (−25 mV), which was comparable to bare UnPSi NPs. These results indicate that the possibility of non-specific adsorption of anti-PSA-NCAM-PE on the surface of UnPSi NPs can be ruled out. Furthermore, the antibody modified NPs anti-PSA-NCAM-UnPSi presented increased stability in the artificial cerebrospinal fluid (ACSF) (Fig. S2).

The surface conjugation of anti-PSA-NCAM-PE to the UnPSi was confirmed using attenuated total reflectance Fourier transform infrared spectroscopy (ATR−FTIR). FTIR is a very sensitive method to determine the surface modification and to identify the functional groups, such as amide, carboxylic acid, aldehyde, ethylene, ethyne, etc. As previously demonstrated, the conjugation of both peptides and polymers to PSi NPs can be detected by FTIR [40–42]. The attenuation of the carbonyl C=O stretching band at 1710 cm^{-1} after the conjugation of anti-PSA-NCAM-PE to UnPSi, was evidenced, along with appearance of the bands at 1635 cm^{-1} and 1532 cm^{-1} corresponding to formation of amide bonds, indicating successful conjugation (Fig. 1e). We have quantified that 4.66 μg of anti-PSA-NCAM-PE were conjugated to 100 μg of UnPSi NPs using fluorescent analysis, which allowed us to calculate the conjugation efficiency of about 45%. Since the anti-PSA-

NCAM is an IgM antibody, excess of free amine groups that exist in the pentameric form facilitated the efficient conjugation process. Furthermore, from the given amount of anti-PSA-NCAM-PE conjugated to the given amount of UnPSi NPs, we estimated that an average of 70 anti-PSA-NCAM-PE molecules were conjugated to the surface of each single UnPSi NP.

Next, we evaluated the cellular interactions of NPs with cultured primary embryonic NSPCs. First, the cytotoxicity of the UnPSi NPs before and after conjugation with anti-PSA-NCAM antibody was tested in cultures of primary embryonic NSPCs at different NP concentrations (25, 50, and 100 μg mL^{-1}) after 6 and 24 h (Fig. S3). Both UnPSi and anti-PSA-NCAM-UnPSi NPs did not shown any significant cytotoxicity at all the tested concentrations suggesting the cytocompatibility of the NPs with embryonic NSPCs, in line with previous publications [32,43].

To investigate the cellular interactions of NPs, anti-PSA-NCAM-PE-UnPSi NP uptake by embryonic NSPCs, containing both NSCs (nestin$^+$) and neuroblasts (PSA-NCAM$^+$ and DCX$^+$) was analyzed by confocal imaging and TEM (Fig. 2a–c). Confocal images confirmed the phenotype of embryonic NSPCs by immunostaining of the cell biomarkers PSA/NCAM, nestin$^+$, and DCX$^+$. (Fig. S4). We observed increased interaction and accumulation of anti-PSA-NCAM-PE-UnPSi NPs in the cells by increasing the concentration of anti-PSA-NCAM-PE-UnPSi NPs, suggesting a concentration-dependent cellular uptake (Fig. 2a). Control UnPSi NPs loaded with tetramethylrhodamine (TRITC) fluorophore did not show any significant interaction with NSPCs even at the highest dose (100 μg ml^{-1}) among the different doses (25, 50 and 100 μg ml^{-1}) tested (Fig. 2a), suggesting negligible nonspecific interaction of non-targeted UnPSi NPs with NSPCs. Flow cytometry analysis showed that NSPCs treated with anti-PSA-NCAM-PE-UnPSi NPs increased the population of cells with high fluorescence intensity, whereas non-targeted UnPSi-TRITC NPs at different concentrations showed lower fluorescence intensity in the cells. All these results suggest that the NP uptake was mediated by the anti-PSA-NCAM antibody (Fig. 2b). Cellular internalization is a critical requirement, particularly if NPs are designed to deliver bioactive molecules and modulate intracellular signaling pathways. In order to analyze whether the anti-PSA-NCAM-PE-UnPSi NPs were internalized by embryonic NSPCs and to gain further insight into their intracellular localization, we visualized the cellular uptake using TEM. After 3 h of incubation, TEM images showed that anti-PSA-NCAM-PE-UnPSi NPs were present in the intracellular regions, while some were found in the endo-/lysosome compartments, and few were present in the cytoplasm of NSPCs (Fig. 2c). Furthermore, we also observed that anti-PSA-NCAM-PE-UnPSi NPs were interacting with the cellular membrane. These results collectively suggest that anti-PSA-NCAM-PE-UnPSi NPs interact with embryonic NSPCs through an antibody-mediated ligand-receptor interaction, which facilitates the cellular internalization via receptor-mediated endocytosis. It should be noted that cellular uptake may be affected by particle size. Often the

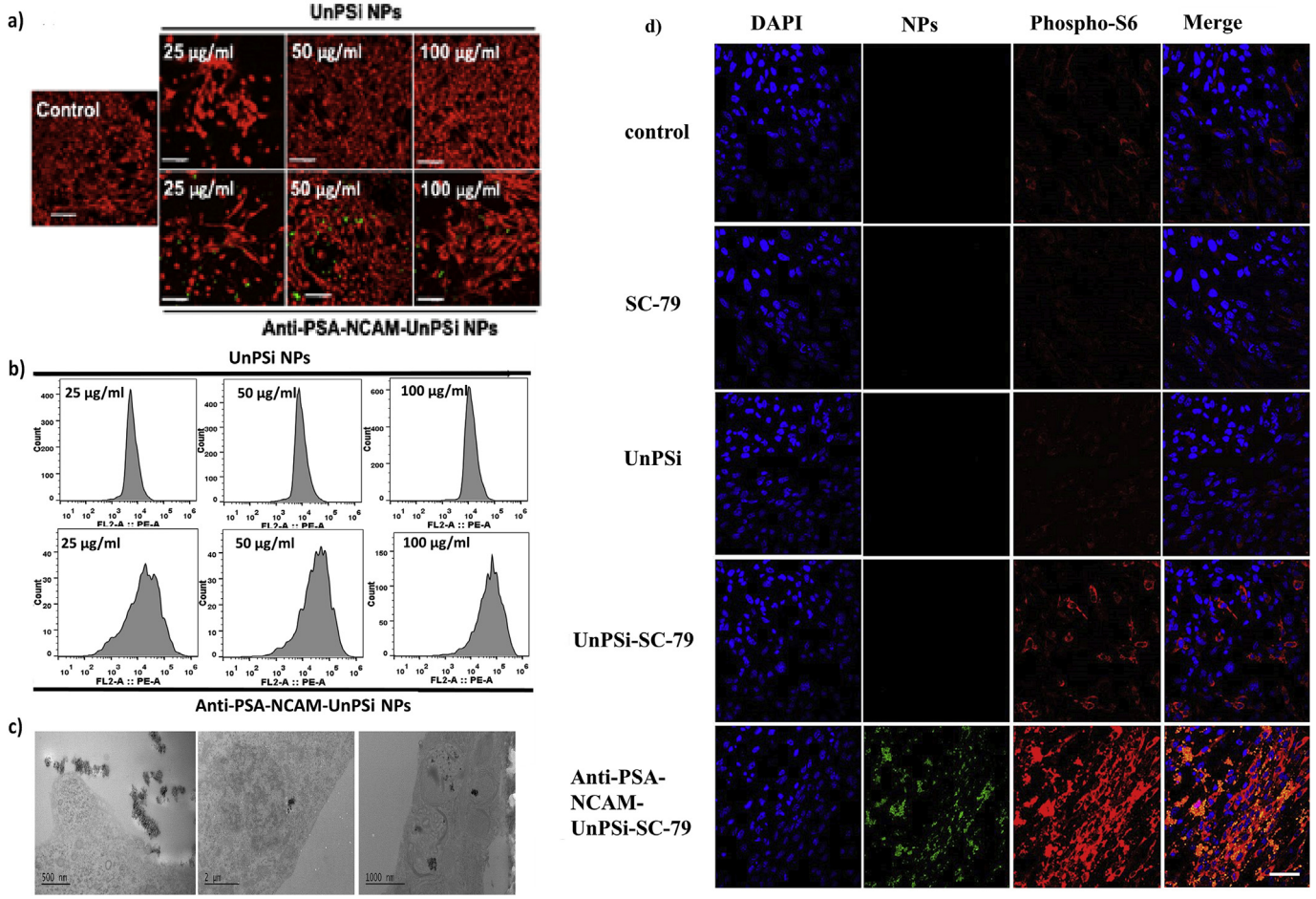

Fig. 2. *In vitro* cellular interaction of NPs and Akt pathway activation after loading SC-79. (a) Confocal images of embryonic NSPCs after 9 h of treatment with non-targeted (UnPSi NPs) and targeted (anti-PSA-NCAM-PE-UnPSi) NPs (red: cell membrane labeled with CellMask DeepRed, green: NPs) at concentrations of 25, 50, and 100 μg/mL. (b) Flow cytometry analysis of cellular uptake of both non-targeted and targeted nanoparticles after 9 h of incubation. (c) TEM images of cellular uptake and intracellular localization of anti-PSA-NCAM-PE-UnPSi NPs in NSPCs after 3 h of incubation. Scale bars are: 500 nm, 2 μm, and 1000 nm. (d) Activation of Akt signaling pathway in NSPCs after 24 h of treatment with free SC-79, non-targeted UnPSi NPs, non-targeted UnPSi NPs loaded with SC-79, and anti-PSA-NCAM-PE-UnPSi NPs loaded with SC-79 (blue: DAPI (cell nuclei), green: PE (NPs); red: phospho-S6). Scale bar: 100 μm (same for all images). (For interpretation of the references to colour in this figure legend, the reader is referred to the Web version of this article.)

particle size plays an important role regarding passive cellular uptake, when the particle size is in the range of less than 200 nm and that smaller NPs have better cellular uptake [44]. In our study, the NPs before and after modification are around 200 and 350 nm, respectively. Furthermore, the increasing particle size after antibody modification is a drawback for cellular uptake. However, our results show that antibody modification increased the cellular interaction and the improvement by the antibody-mediated internalization is so significant that the effect due to the size is not dominant.

Akt pathway activation plays an important role in mediating cell survival and preventing apoptosis of different neuronal populations [45]. A small molecule, SC-79, has been identified as a potent Akt pathway activator in different cells [29]. SC-79 binds the pleckstrin homology region of Akt, thereby enhancing Akt phosphorylation and activating the Akt signaling pathway. Thus, to promote survival of the targeted endogenous neuroblasts, we loaded SC-79 in anti-PSA-NCAM-PE-UnPSi NPs and analyzed their efficiency to activate the Akt pathway in embryonic NSPCs. From the quantitative analysis of SC-79 loading in anti-PSA-NCAM-PE-UnPSi NPs using high-performance liquid chromatography, we calculated that 30 μg of SC-79 were loaded in 100 μg of anti-PSA-NCAM-PE-UnPSi NPs, corresponding to a loading degree of 23% (wt-%). SC-79 was utilized as the only commercially available drug stimulating Akt pathway; during the course of the experiments we have found out its low stability in aqueous solutions. Confocal images showed that after 24 h of incubation, the SC-79 loaded anti-PSA-NCAM-PE-UnPSi NPs extensively activated the Akt pathway (detected by the immunofluorescent staining for phospho-S6 ribosomal protein) in NSPCs at all the NP doses tested (25, 50, 100 μg ml^{-1}), compared to different controls (free SC-79, non-targeted UnPSi and non-targeted UnPSi NPs loaded with SC-79) (Fig. 2d). These results demonstrate that internalized anti-PSA-NCAM-PE-UnPSi NPs can deliver the SC-79 intracellularly and modulate the Akt signaling pathway in NSPCs. Moreover, these data also show that the NPs with antibody modification still had better cellular uptake and drug delivery efficiency after the short time immerging in the solution of DMSO/ethanol during SC-79 loading.

In order to demonstrate the feasibility of targeting of PSA-$NCAM^+$ neuroblasts *in vivo* after systemic administration, anti-PSA-NCAM-PE-UnPSi NPs were radiolabeled with iodine-125 ($t_{1/2}$ = 59.408 d, E_γ = 35.4919 keV), and the *ex vivo* biodistribution and capability of the nanovector to extravasate to the brain was evaluated in a rat surgical model of ischemic stroke. In the model, a stroke is induced by a 60-min ligation of the bilateral common carotid arteries (CAA) and the right middle cerebral artery (MCA), and the procedure results in impairment of the blood-brain barrier (BBB) at the ischemic hemisphere [35]. Therefore, we postulated that the anti-PSA-NCAM-PE NPs might pass

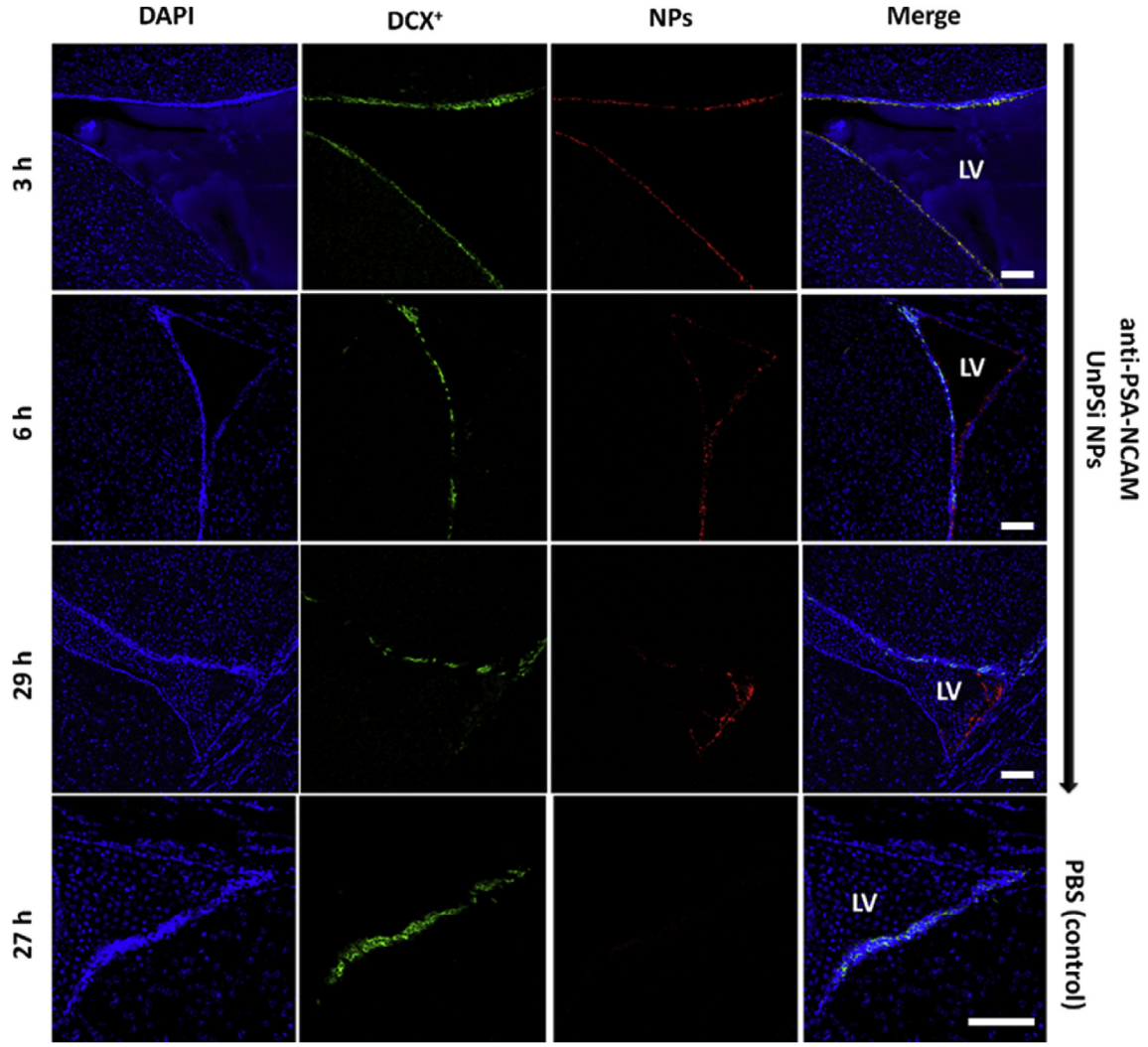

Fig. 3. *In vivo* targeting and accumulation of anti-PSA-NCAM-PE-UnPSi NPs to DCX^+ neuroblasts in SVZ. Confocal images of mouse brain sections at different time points after local bilateral intraventricular injections of anti-PSA-NCAM-PE-UnPSi NPs (blue: DAPI (cell nuclei); green: DCX^+ neuroblasts; red: PE (NPs)). Scale bar: 200 μm (same to all images). (For interpretation of the references to colour in this figure legend, the reader is referred to the Web version of this article.)

the BBB passively in the stroke model, and could then be used to target to the endogenous neuroblasts expressing NCAM and DCX in the SVZ *in vivo*. Anti-PSA-NCAM-PE-UnPSi NPs were successfully labeled with ^{125}I to the tyrosine residues of the anti-PSA-NCAM-PE antibody using Chloramine-T as an oxidizer with 59–65% radiochemical yield, radiochemical purity of 97.7–98.6%, and specific radioactivity ranging from 91.3 to 121.7 MBq mg^{-1} (n = 2). The radiolabel was stable in the formulated solution (1 × PBS, pH 7.4) and in physiological conditions (50% human plasma) with over 93% of the radiolabel remaining in the NPs after 6 h of incubation (Fig. S5). After intravenous administration to the stroke model rats (48 h post-surgery) and to operation-naïve controls, the biodistribution of the ^{125}I-labeled anti-PSA-NCAM-PE-UnPSi NPs was determined by *ex vivo* radioactivity measurements of excised tissues at 2 h and 24 h after NP administration. Systemically administered ^{125}I-labeled anti-PSA-NCAM-PE-UnPSi NPs showed maximum signal in the brain at 2 h post injection (p.i.), but with prominent accumulation to the liver and spleen, the principal organs of the reticulo-endothelial system (RES). There was a ca. 2-fold statistically significant increase in the ^{125}I signal in the stroke hemisphere compared to the signal in either the contralateral non-operated hemisphere in the same animal or the corresponding hemisphere in the operation-naïve control (Fig. S6), suggesting that BBB penetration of the ^{125}I-labeled anti-PSA-NCAM-PE-UnPSi NPs is feasible. At 2 h p.i., the degree of dehalogenation *in vivo* was comparable to that reported for radioiodinated monoclonal antibodies [46] (Fig. S7a), but at the later time point, at 24 h p.i., the radioactivity signal in the thyroid (indicative of dehalogenation *in vivo*) exceeded that typically reported for radioiodinated bioconjugates, which is unsurprising given the high enzymatic activity in the liver and the accumulation of the NPs there (Fig. S7b). Since it was clear from these results that the systemic bioavailability to the brain of the anti-PSA-NCAM-PE-UnPSi NPs was limited, the targeting efficacy of anti-PSA-NCAM conjugated UnPSi NPs was further evaluated through local bilateral intraventricular injections. To improve the ability of the construct to evade immune recognition and RES clearance an intracranial approach was warranted.

To investigate the potential of anti-PSA-NCAM-PE-UnPSi NPs to target endogenous neuroblasts expressing DCX in SVZ *in vivo* after intracranial injection, the anti-PSA-NCAM-PE-UnPSi NPs were stereotaxically injected bilaterally to the lateral ventricles (LVs) of adult (8–10 weeks old) mice. After dissecting the brains at different time points (3, 6, and 29 h p.i.), brain sections were analyzed using immunofluorescent staining for DCX and confocal microscopy. At 3 h p.i., the majority of the injected anti-PSA-NCAM-PE-UnPSi NPs accumulated around the walls of the LVs, which might be due to the increased initial accumulation of the NPs in the confined LV and most of them were co-localized with DCX$^+$ neuroblasts in the SVZ (Fig. 3 and Fig. S8). However, over time (6 and 29 h p.i.), the amount of accumulated anti-PSA-NCAM-PE-UnPSi NPs around the walls of LVs was reduced, probably due to the flow of cerebrospinal fluid, which washed away the unattached or loosely adsorbed anti-PSA-NCAM-PE-UnPSi NPs.

At 29 h p.i., only anti-PSA-NCAM-PE-UnPSi NPs that interacted with or were taken up by the cells were still present next to the walls of the LVs and in the SVZ (Fig. 3). Interestingly, other controls UnPSi-TRITC NPs and physically mixed anti-PSA-NCAM-PE with UnPSi NPs (simulated conjugation conditions) were not significantly visible in the walls of the LVs or the SVZ (Fig. S9). Co-localization signal from anti-PSA-NCAM-PE-UnPSi NPs and DCX$^+$ neuroblasts indicates the specificity of the anti-PSA-NCAM-PE-UnPSi NPs to target DCX$^+$ neuroblasts in the SVZ.

Furthermore, we investigated the potential of targeted delivery of SC-79 by anti-PSA-NCAM-PE-UnPSi NPs to stimulate the Akt pathway in endogenous DCX$^+$ neuroblasts in the SVZ. Confocal and immunofluorescent imaging analysis of the brain sections obtained from mice treated with SC-79 loaded anti-PSA-NCAM-PE-UnPSi NPs (0.5 μg per LV, corresponding to 0.15 μg per LV of loaded SC-79) and other controls revealed that the SC-79 loaded anti-PSA-NCAM-PE-UnPSi NPs can

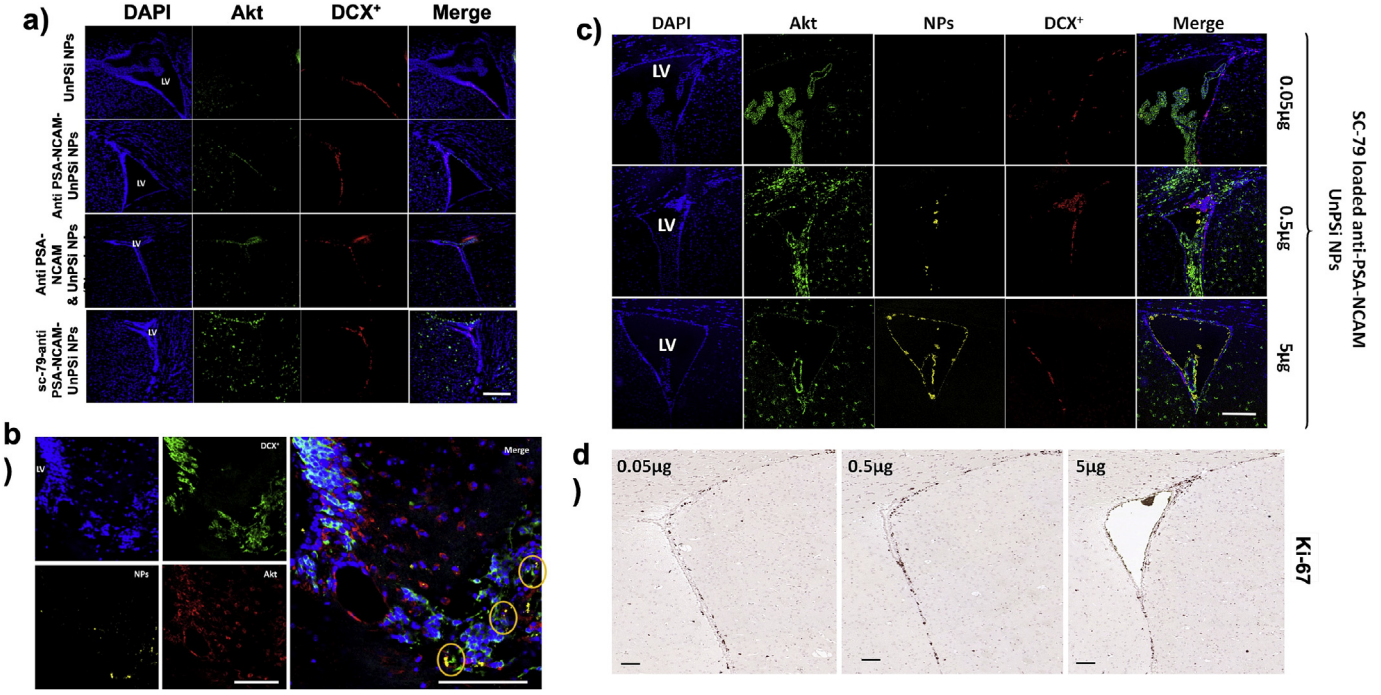

Fig. 4. *In vivo* analysis of targeted nanoparticle-mediated Akt pathway activation and cell proliferation. (a) Mouse brain sections 24 h after local bilateral intraventricular injections of the SC-79 loaded anti-PSA-NCAM-PE-UnPSi NPs compared with other controls (blue: DAPI (cell nuclei), green: phospho-S6, red: DCX$^+$ neuroblasts). (b) Triple co-localization of SC-79 loaded anti-PSA-NCAM-PE-UnPSi NPs with DCX$^+$ neuroblasts in the SVZ and Akt pathway activation (blue: DAPI (cell nuclei), green: DCX$^+$ neuroblasts, yellow: NPs, red: phospho-S6). (c) Confocal and immunofluorescence analysis of targeting and Akt pathway activation in DCX$^+$ neuroblasts in the SVZ with different doses (blue: DAPI (cell nuclei), green: phospho-S6, yellow: NPs, red: DCX$^+$ neuroblasts). (d) Cellular proliferation analysis in the SVZ and the striatum using anti-Ki67 immunostaining. Scale bar: 200 μm (a, c and d), the same to all images; 100 μm (b). (For interpretation of the references to colour in this figure legend, the reader is referred to the Web version of this article.)

stimulate the Akt pathway (evidenced by phospho-S6 immunostaining) in the SVZ, compared to other controls (non-targeted UnPSi NPs, physically mixed anti-PSA-NCAM-PE/UnPSi NPs, anti-PSA-NCAM-PE and UnPSi NPs without SC-79) (Fig. 4a). In addition, the triple co-localization of the anti-PSA-NCAM-PE-UnPSi NPs, DCX^+ neuroblasts and Akt activation marker phospho-S6 showed that the anti-PSA-NCAM-PE-UnPSi NPs can target endogenous DCX^+ neuroblasts in the SVZ and *in situ* stimulate the activation of the Akt pathway (Fig. 4b). However, we have also observed phospho-S6 immunostaining in other cells in the striatum lateral to the SVZ, which was possibly due to the facilitated diffusion of SC-79 released from the accumulated NPs.

To further demonstrate the *in vivo* targeting and stimulation of the Akt signaling pathway in endogenous DCX^+ neuroblasts in the SVZ, we evaluated the dose-dependent effects *in vivo* using different concentrations of the SC-79 loaded anti-PSA-NCAM-PE-UnPSi NPs (0.05, 0.5, and 5 μg per LV), corresponding to the different doses of loaded SC-79 (0.015, 0.15, 1.5 μg per LV), respectively. We observed that the anti-PSA-NCAM-PE-UnPSi NPs at high doses (5 μg per LV) were not able to diffuse deep into the brain parenchyma from the LVs, as the diffusion was limited to the ependymal/sub-ependymal layer (Fig. 4c, bottom row). As the concentration can influence the aggregation, it may be that larger aggregates of the NPs may remain trapped in those layers, limiting their further diffusion. At the intermediate dose (0.5 μg/LV), anti-PSA-NCAM-PE-UnPSi NPs aggregated significantly less than with the highest dose, which in turn led to improved dispersion and diffusion and, as a result, we observed that anti-PSA-NCAM-PE-UnPSi NPs could diffuse further and target DCX^+ neuroblasts in the SVZ (Fig. 4c, middle row). Nevertheless, at the lowest dose (0.05 μg), we did not observe a significant amount of the anti-PSA-NCAM-PE-UnPSi NPs in the walls of the LVs and in DCX^+ neuroblasts in the SVZ (Fig. 4c, top row). Altogether, these results demonstrate that optimizing the concentration of the anti-PSA-NCAM-PE-UnPSi NPs is crucial for effective *in vivo* targeting, where high concentration may cause aggregation and low concentration may not be sufficient to achieve effective targeting.

To evaluate whether activating the Akt pathway in neuroblasts can enhance their proliferation, we analyzed the immunostaining with anti-Ki67 proliferation marker antibody in mouse brain sections after treatment with different doses of the SC-79 loaded anti-PSA-NCAM-PE-UnPSi NPs. To ensure the occurrence of the Akt activation, we used the brain sections from the same mice that were showing the dose dependent Akt activation (Fig. 4c). We did not observe any significant increase in cell proliferation neither in DCX^+ neuroblasts nor in other cells in the striatum (Fig. 4d).

Overall, targeting endogenous neuroblasts to promote their survival may stimulate neuronal differentiation to generate more functional neurons. This potentially has therapeutic benefits for the treatment of stroke where survival of migrating neuroblasts is promoted. Here, we demonstrate for the first time that NPs can target endogenous neuroblasts and stimulate the neuron survival signaling pathway both *in vitro* and *in vivo*. The phosphatidylinositol-3-kinase (PI3K)/Akt signaling pathway regulates NSC proliferation and differentiation, and neuroblast migration [47]. Akt pathway activation can stimulate several anti-apoptotic pathways [48] and protect neurons *in vivo* [49,50]. Small molecule compound SC-79 can bind to Akt and facilitate its phosphorylation by upstream protein kinases, stimulating neuronal survival in a mouse stroke model [29]. However, aberrant activation of the Akt pathway also promotes carcinogenesis and is frequently associated with malignancy [51]. In fact, Akt signaling inhibitors are considered as promising agents for cancer therapy [51,52]. Thus, despite beneficial effects in neurodegeneration treatment, non-targeted delivery of Akt pathway stimulating drugs may considerably increase the risk of cancer and therefore have limited therapeutic applicability. In contrast, our results demonstrate that activating the Akt pathway in neuroblasts in the SVZ using drug-loaded targeted NPs did not induce cell proliferation.

Interestingly, we observed a correlation between the concentration dependent NP accumulation and *in situ* stimulation of the Akt pathway. As suggested above, a higher dose of NPs (5 μg per LV) induced aggregation and larger NP aggregates were trapped in the first ependymal layer present next to the walls of the LVs, whereas an intermediate NP dose (0.5 μg per LV) was relatively well dispersed and diffused more in the SVZ and co-localized with DCX^+ neuroblasts. Therefore, although the intermediate dose of SC-79 (0.15 μg per LV) was 10 times less than the high dose (1.5 μg per LV), the increased diffusion in the SVZ due to the improved dispersion (reduced aggregation behavior) of NPs activated the Akt pathway much more than the other doses tested. However, there was also Akt activation in the striatum, further way from the SVZ. As we did not observe any NPs in the striatum (beyond the SVZ), the SC-79 loaded anti-PSA-NCAM-PE-UnPSi NPs that accumulated in the SVZ may have served as a depot of SC-79 that was most likely released from the NPs and diffused to the neighboring brain areas. It is worth noting that the lowest dose of NPs (0.05 μg per LV) and the corresponding low dose of loaded SC-79 (0.015 μg per LV) were not sufficient to target the endogenous DCX^+ neuroblasts, and thus, ultimately did not stimulate the activation of Akt signaling in the SVZ.

In the present proof-of-principle study, we aimed to demonstrate the ability of antibody-conjugated NPs to target NSPCs in culture and *in vivo* following systemic administration after stroke. We also show that antibody-conjugated NPs can be loaded with a drug, and SC-79 was utilized as the only commercially available drug stimulating the Akt pathway. To demonstrate functional outcome of the treatment, several hurdles have to be overcome. First, diffusion of NPs in the brain parenchyma has to be improved. Second, SC-79 is far from an optimal drug for NP loading due to its limited stability and the ability to leak from NPs, which can lead to unspecific targeting of neighboring cells. Third, penetration to the brain after stroke, though detectable, will likely not be sufficient to observe any behavioral and/or functional effects. The specificity of NP targeting should also be studied further, most importantly, in *in vivo* settings. Further optimization of the system is required to address these issues, as well as to improve efficacy of BBB penetration, diffusion and targeting. Most stem-cell based therapeutic strategies to treat neurodegenerative diseases and other brain disorders associated with neuronal injuries are focused on either direct exogenous transplantation of NSCs or stimulating proliferation and differentiation of endogenous NSCs to generate new neurons [4]. However, controlling the proliferation and directed differentiation of NSCs to functional neurons able to integrate into existing neuronal networks is extremely challenging. Furthermore, NSC-based therapeutic approaches raise the concern of stimulating carcinogenesis due to the possible uncontrolled proliferation of NSCs. Considering that neuroblasts are committed neuronal progenitors with a limited proliferation potential, targeting endogenous neuroblasts can be an ideal choice to stimulate neuronal differentiation. We therefore will focus our further studies to prevent uncontrolled release of the loaded drug, find optimal concentrations, improve specificity and brain diffusion properties of targeted NPs, and demonstrate increased neurogenesis after treatment with neuroblast-targeting drug-loaded NPs *in vivo* in a rodent model of stroke.

It should be noted that endogenous neurogenesis after stroke is rather limited [53] and is restricted to specific small regions in the brain. However, our results and approach can be implemented in neural stem cell transplantation studies after stroke, in this case NPs could be injected together with transplanted cells to stimulate cell survival and differentiation. We envision that the approach could also be used in parallel with parenchymal glial cell reprogramming, where glial cells are converted to neurons using viral vectors [54]. These treatments can also be combined with replacing dead tissue with ECM hydrogel [55,56].

This study opens up new avenues to target the endogenous neuroblasts with NPs and stimulate their intracellular pathways supporting survival and neuronal differentiation and adult neurogenesis, which will potentially benefit the development of new therapeutic strategies

aiming at replacing neuronal circuitry after stroke.

Data availability

All of the data reported in this work are available upon request.

Declaration of competing interest

The authors declare that there are no conflicts of interest in this work.

Acknowledgements

We thank Ms Congjun Zheng and Ms Neha Pratap Singh for primary cell cultures and Ms Marjo Vaha for the technical support with the *ex vivo* biodistribution study in the rat stroke model. We also thank Ms Charlotte Zeitler for cutting the brain sections. The financial support from the Tekes large strategic research opening 3iRegeneration (project no. 40395/13) is gratefully acknowledged. A. Domanskyi was supported by the Academy of Finland (grants nos. 293392 and 287843). M. Sarparanta, O. Alanen and A.J. Airaksinen were supported by the Academy of Finland (grant nos. 278056 and 298481). M. Airavaara was supported by Academy of Finland (grants nos. 250275, 256398, 281394, and 309489). H.A. Santos acknowledges financial support from the HiLIFE Research Funds, the Sigrid Jusélius Foundation, and the European Research Council Proof-of-Concept Research Grant (grant no. 825020). We also thank Katrina Albert for proof-reading our paper. The authors also acknowledge the following core facilities funded by Biocenter Finland: Electron Microscopy Unit of the University of Helsinki for providing the facilities for TEM imaging, the Light Microscopy Unit of the Institute of Biotechnology for providing confocal microscopy facilities and the Radiopharmaceutical chemistry facility of the University of Helsinki.

Appendix A. Supplementary data

Supplementary data to this article can be found online at https://doi.org/10.1016/j.biomaterials.2019.119556.

References

[1] A. Alvarez-Buylla, D.A. Lim, For the long run: maintaining germinal niches in the adult brain, Neuron 41 (2004) 683–686.
[2] K.A. Sailor, G.L. Ming, H. Song, Neurogenesis as a potential therapeutic strategy for neurodegenerative diseases, Expert Opin. Biol. Ther. 6 (2006) 879–890.
[3] Fred H. Gage, S. Temple, Neural stem cells: generating and regenerating the brain, Neuron 80 (2013) 588–601.
[4] S.E. Latchney, A.J. Eisch, Therapeutic application of neural stem cells and adult neurogenesis for neurodegenerative disorders: regeneration and beyond, Eur. J. Neurodegener. Dis. 1 (2012) 335–351.
[5] F. Rossi, E. Cattaneo, Neural stem cell therapy for neurological diseases: dreams and reality, Nat. Rev. Neurosci. 3 (2002) 401–409.
[6] D. Carradori, J. Eyer, P. Saulnier, V. Préat, A. des Rieux, The therapeutic contribution of nanomedicine to treat neurodegenerative diseases via neural stem cell differentiation, Biomaterials 123 (2017) 77–91.
[7] M. Warashina, K.H. Min, T. Kuwabara, A. Huynh, F.H. Gage, P.G. Schultz, S. Ding, A synthetic small molecule that induces neuronal differentiation of adult hippocampal neural progenitor cells, Angew. Chem. Int. Ed. 45 (2006) 591–593.
[8] Y. Ning, J. Huang, B. Kalionis, Q. Bian, J. Dong, J. Wu, X. Tai, S. Xia, Z. Shen, Oleanolic Acid induces differentiation of neural stem cells to neurons: an involvement of transcription factor Nkx-2.5, Stem Cell. Int. 2015 (2015) 12.
[9] H.E. Marei, A. Hasan, R. Rizzi, A. Althani, N. Afifi, C. Cenciarelli, T. Caceci, A. Shuaib, Potential of stem cell-based therapy for ischemic stroke, Front. Neurol. 9 (2018) 34.
[10] K.-Y. Tseng, J.E. Anttila, K. Khodosevich, R.K. Tuominen, M. Lindahl, A. Domanskyi, M. Airavaara, MANF promotes differentiation and migration of neural progenitor cells with potential neural regenerative effects in stroke, Mol. Ther. 26 (2018) 238–255.
[11] V.P. Torchilin, Multifunctional, stimuli-sensitive nanoparticulate systems for drug delivery, Nat. Rev. Drug Discov. 13 (2014) 813–827.
[12] S. Mitragotri, P.A. Burke, R. Langer, Overcoming the challenges in administering biopharmaceuticals: formulation and delivery strategies, Nat. Rev. Drug Discov. 13 (2014) 655–672.
[13] R.A. Petros, J.M. DeSimone, Strategies in the design of nanoparticles for therapeutic applications, Nat. Rev. Drug Discov. 9 (2010) 615–627.
[14] N. Kamaly, Z. Xiao, P.M. Valencia, A.F. Radovic-Moreno, O.C. Farokhzad, Targeted polymeric therapeutic nanoparticles: design, development and clinical translation, Chem. Soc. Rev. 41 (2012) 2971–3010.
[15] Y. Min, J.M. Caster, M.J. Eblan, A.Z. Wang, Clinical translation of nanomedicine, Chem. Rev. 115 (2015) 11147–11190.
[16] R. Misra, S. Acharya, S.K. Sahoo, Cancer nanotechnology: application of nanotechnology in cancer therapy, Drug Discov. Today 15 (2010) 842–850.
[17] C. Saraiva, C. Praça, R. Ferreira, T. Santos, L. Ferreira, L. Bernardino, Nanoparticle-mediated brain drug delivery: overcoming blood–brain barrier to treat neurodegenerative diseases, J. Control. Release 235 (2016) 34–47.
[18] T. Santos, J. Maia, F. Agasse, S. Xapelli, L. Ferreira, L. Bernardino, Nanomedicine boosts neurogenesis: new strategies for brain repair, Integr Biol (Camb) 4 (2012) 973–981.
[19] T. Santos, R. Ferreira, J. Maia, F. Agasse, S. Xapelli, L. Cortes, J. Bragança, J.O. Malva, L. Ferreira, L. Bernardino, Polymeric nanoparticles to control the differentiation of neural stem cells in the subventricular zone of the brain, ACS Nano 6 (2012) 10463–10474.
[20] D. Carradori, P. Saulnier, V. Preat, A. des Rieux, J. Eyer, NFL-lipid nanocapsules for brain neural stem cell targeting in vitro and in vivo, J. Control. Release 238 (2016) 253–262.
[21] F.H. Gage, Mammalian neural stem cells, Science 287 (2000) 1433–1438.
[22] G.L. Ming, H. Song, Adult neurogenesis in the mammalian brain: significant answers and significant questions, Neuron 70 (2011) 687–702.
[23] S. Temple, The development of neural stem cells, Nature 414 (2001) 112–117.
[24] N. Amariglio, A. Hirshberg, B.W. Scheithauer, Y. Cohen, R. Loewenthal, L. Trakhtenbrot, N. Paz, M. Koren-Michowitz, D. Waldman, L. Leider-Trejo, A. Toren, S. Constantini, G. Rechavi, Donor-derived brain tumor following neural stem cell transplantation in an ataxia telangiectasia patient, PLoS Med. 6 (2009) e1000029.
[25] A. Trounson, N.D. DeWitt, Pluripotent stem cells progressing to the clinic, Nat. Rev. Mol. Cell Biol. 17 (2016) 194–200.
[26] G. Friocourt, J.S. Liu, M. Antypa, S. Rakic, C.A. Walsh, J.G. Parnavelas, Both doublecortin and doublecortin-like kinase play a role in cortical interneuron migration, J. Neurosci. 27 (2007) 3875–3883.
[27] E. Gascon, L. Vutskits, B. Jenny, P. Durbec, J.Z. Kiss, PSA-NCAM in postnatally generated immature neurons of the olfactory bulb: a crucial role in regulating p75 expression and cell survival, Development (Camb.) 134 (2007) 1181–1190.
[28] R. Filipovic, S. Santhosh Kumar, C. Fiondella, J. Loturco, Increasing doublecortin expression promotes migration of human embryonic stem cell-derived neurons, Stem Cells 30 (2012) 1852–1862.
[29] H. Jo, S. Mondal, D. Tan, E. Nagata, S. Takizawa, A.K. Sharma, Q. Hou, K. Shanmugasundaram, A. Prasad, J.K. Tung, A.O. Tejeda, H. Man, A.C. Rigby, H.R. Luo, Small molecule-induced cytosolic activation of protein kinase Akt rescues ischemia-elicited neuronal death, Proc. Natl. Acad. Sci. U.S.A. 109 (2012) 10581–10586.
[30] H.A. Santos, E. Mäkilä, A.J. Airaksinen, L.M. Bimbo, J. Hirvonen, Porous silicon nanoparticles for nanomedicine: preparation and biomedical applications, Nanomedicine 9 (2014) 535–554.
[31] L.M. Bimbo, M. Sarparanta, H.A. Santos, A.J. Airaksinen, E. Mäkilä, T. Laaksonen, L. Peltonen, V.-P. Lehto, J. Hirvonen, J. Salonen, Biocompatibility of thermally hydrocarbonized porous silicon nanoparticles and their biodistribution in rats, ACS Nano 4 (2010) 3023–3032.
[32] M.-A. Shahbazi, M. Hamidi, E.M. Mäkilä, H. Zhang, P.V. Almeida, M. Kaasalainen, J.J. Salonen, J.T. Hirvonen, H.A. Santos, The mechanisms of surface chemistry effects of mesoporous silicon nanoparticles on immunotoxicity and biocompatibility, Biomaterials 34 (2013) 7776–7789.
[33] W. Li, Z. Liu, F. Fontana, Y. Ding, D. Liu, J.T. Hirvonen, H.A. Santos, Tailoring porous silicon for biomedical applications: from drug delivery to cancer immunotherapy, Adv. Mater. 30 (2018) e1703740.
[34] M.A. Tölli, M.P. Ferreira, S.M. Kinnunen, J. Rysa, E.M. Mäkilä, Z. Szabo, R.E. Serpi, P.J. Ohukainen, M.J. Valimäki, A.M. Correia, J.J. Salonen, J.T. Hirvonen, H.J. Ruskoaho, H.A. Santos, In vivo biocompatibility of porous silicon biomaterials for drug delivery to the heart, Biomaterials 35 (2014) 8394–8405.
[35] K. Mätlik, J.E. Anttila, T. Kuan-Yin, O.-P. Smolander, E. Pakarinen, L. Lehtonen, U. Abo-Ramadan, P. Lindholm, C. Zheng, B. Harvey, U. Arumäe, M. Lindahl, M. Airavaara, Poststroke delivery of MANF promotes functional recovery in rats, Sci. Adv. 4 (2018) eaap8957.
[36] C.F. Wang, M.P. Sarparanta, E.M. Mäkilä, M.L. Hyvönen, P.M. Laakkonen, J.J. Salonen, J.T. Hirvonen, A.J. Airaksinen, H.A. Santos, Multifunctional porous silicon nanoparticles for cancer theranostics, Biomaterials 48 (2015) 108–118.
[37] P.J. Kinnari, M.L.K. Hyvönen, E.M. Mäkilä, M.H. Kaasalainen, A. Rivinoja, J.J. Salonen, J.T. Hirvonen, P.M. Laakkonen, H.A. Santos, Tumour homing peptide-functionalized porous silicon nanovectors for cancer therapy, Biomaterials 34 (2013) 9134–9141.
[38] M. Kovalainen, J. Mönkäre, E. Makila, J. Salonen, V.P. Lehto, K.H. Herzig, K. Järvinen, Mesoporous silicon (PSi) for sustained peptide delivery: effect of psi microparticle surface chemistry on peptide YY3-36 release, Pharm. Res. 29 (2012) 837–846.
[39] R. Saber, S. Sarkar, P. Gill, B. Nazari, F. Faridani, High resolution imaging of IgG and IgM molecules by scanning tunneling microscopy in air condition, Sci. Iran. 18 (2011) 1643–1646.
[40] C.-F. Wang, E.M. Mäkilä, C. Bonduelle, J. Rytkönen, J. Raula, S. Almeida, A. Närvänen, J.J. Salonen, S. Lecommandoux, J.T. Hirvonen, H.A. Santos, Functionalization of alkyne-terminated thermally hydrocarbonized porous silicon

nanoparticles with targeting peptides and antifouling polymers: effect on the human plasma protein adsorption, ACS Appl. Mater. Interfaces 7 (2015) 2006–2015.
[41] C.-F. Wang, E.M. Mäkilä, M.H. Kaasalainen, D. Liu, M.P. Sarparanta, A.J. Airaksinen, J.J. Salonen, J.T. Hirvonen, H.A. Santos, Copper-free azide–alkyne cycloaddition of targeting peptides to porous silicon nanoparticles for intracellular drug uptake, Biomaterials 35 (2014) 1257–1266.
[42] P.V. Almeida, M.A. Shahbazi, E. Mäkilä, M. Kaasalainen, J. Salonen, J. Hirvonen, H.A. Santos, Amine-modified hyaluronic acid-functionalized porous silicon nanoparticles for targeting breast cancer tumors, Nanoscale 6 (2014) 10377–10387.
[43] M.P. Ferreira, S. Ranjan, A.M. Correia, E.M. Mäkilä, S.M. Kinnunen, H. Zhang, M.A. Shahbazi, P.V. Almeida, J.J. Salonen, H.J. Ruskoaho, A.J. Airaksinen, J.T. Hirvonen, H.A. Santos, In vitro and in vivo assessment of heart-homing porous silicon nanoparticles, Biomaterials 94 (2016) 93–104.
[44] M. Airavaara, M.H. Voutilainen, Y. Wang, B. Hoffer, Neurorestoration, Park. Relat. Disord. 18 (Suppl 1) (2012) S143–S146.
[45] M.R. Aburto, M. Magarinos, Y. Leon, I. Varela-Nieto, H. Sanchez-Calderon, AKT signaling mediates IGF-I survival actions on otic neural progenitors, PLoS One 7 (2012) e30790.
[46] D.F. Hayes, M.R. Zalutsky, W. Kaplan, M. Noska, A. Thor, D. Colcher, D.W. Kufe, Pharmacokinetics of radiolabeled monoclonal antibody b6.2 in patients with metastatic breast cancer, Cancer Res. 46 (1986) 3157.
[47] S.H. Koh, E.H. Lo, The role of the PI3K Pathway in the regeneration of the damaged brain by neural stem cells after cerebral infarction, J. Clin. Neurol. 11 (2015) 297–304.
[48] A. Brunet, S.R. Datta, M.E. Greenberg, Transcription-dependent and -independent control of neuronal survival by the PI3K-Akt signaling pathway, Curr. Opin. Neurobiol. 11 (2001) 297–305.
[49] V. Ries, C. Henchcliffe, T. Kareva, M. Rzhetskaya, R. Bland, M.J. During, N. Kholodilov, R.E. Burke, Oncoprotein Akt/PKB induces trophic effects in murine models of Parkinson's disease, Proc. Natl. Acad. Sci. U.S.A. 103 (2006) 18757–18762.
[50] A. Domanskyi, C. Geissler, I.A. Vinnikov, H. Alter, A. Schober, M.A. Vogt, P. Gass, R. Parlato, G. Schutz, Pten ablation in adult dopaminergic neurons is neuroprotective in Parkinson's disease models, FASEB J. 25 (2011) 2898–2910.
[51] K. Mahajan, N.P. Mahajan, PI3K-independent AKT activation in cancers: a treasure trove for novel therapeutics, J. Cell. Physiol. 227 (2012) 3178–3184.
[52] C. Porta, C. Paglino, A. Mosca, Targeting PI3K/Akt/mTOR signaling in cancer, Front. Oncol. 4 (2014) 64.
[53] K.Y. Tseng, J.E. Anttila, K. Khodosevich, R.K. Tuominen, M. Lindahl, A. Domanskyi, M. Airavaara, MANF promotes differentiation and migration of neural progenitor cells with potential neural regenerative effects in stroke, Mol. Ther. 26 (2018) 238–255.
[54] P. Arlotta, B. Berninger, Brains in metamorphosis: reprogramming cell identity within the central nervous system, Curr. Opin. Neurobiol. 27 (2014) 208–214.
[55] H. Ghuman, C. Mauney, J. Donnelly, A.R. Massensini, S.F. Badylak, M. Modo, Biodegradation of ECM hydrogel promotes endogenous brain tissue restoration in a rat model of stroke, Acta Biomater. 80 (2018) 66–84.
[56] H. Ghuman, M. Gerwig, F.J. Nicholls, J.R. Liu, J. Donnelly, S.F. Badylak, M. Modo, Long-term retention of ECM hydrogel after implantation into a sub-acute stroke cavity reduces lesion volume, Acta Biomater. 63 (2017) 50–63.